Journal of Magnetism and Magnetic Materials 322 (2010) 3396–3400

Contents lists available at ScienceDirect

Journal of Magnetism and Magnetic Materials

journal homepage: www.elsevier.com/locate/jmmm

Cation distribution dependence of magnetic properties of sol–gel prepared $MnFe_2O_4$ spinel ferrite nanoparticles

Jianjun Li [a], Hongming Yuan [b], Guodong Li [b], Yanju Liu [c], Jinsong Leng [a,*]

[a] Centre for Composite Materials and Structures, Harbin Institute of Technology, Harbin 150001, PR China
[b] State Key Laboratory of Inorganic Synthesis and Preparative Chemistry, College of Chemistry, Jilin University, Changchun 130012, PR China
[c] Department of Aerospace Science and Technology, Harbin Institute of Technology, Harbin 150001, PR China

ARTICLE INFO

Article history:
Received 3 January 2010
Received in revised form
9 June 2010
Available online 18 June 2010

Keywords:
$MnFe_2O_4$ nanoparticle
Particle size
Initial magnetic susceptibility
Cation distribution

ABSTRACT

$MnFe_2O_4$ nanoparticles have been synthesized with a sol–gel method. Both differential thermal and thermo-gravimetric analyses indicate that $MnFe_2O_4$ nanoparticles form at 400 °C. Samples treated at 450 and 500 °C exhibit superparamagnetism at room temperature as implied from vibrating sample magnetometry. Mössbauer results indicate that as Mn^{2+} ions enter into the octahedral sites, Fe^{3+} ions transfer from octahedral to tetrahedral sites. When the calcination temperature increases from 450 to 700 °C, the occupation ratio of Fe^{3+} ions at the octahedral sites decreases from 43% to 39%. Susceptibility measurements versus magnetic field are reported for various temperatures (from 450 to 700 °C) and interpreted within the Stoner–Wohlfarth model.

1. Introduction

Nanosize magnetic oxides have attracted considerable interest for their wide applications ranging from fundamental research to industrial applications. Spinel ferrite, MFe_2O_4 (M=Mn, Co, Zn, Mg, etc.), is one of the most important magnetic oxides, where oxygen has fcc close packing and M^{2+} and Fe^{3+} ions can occupy either tetrahedral (A) or octahedral (B) interstitial sites [1]. The spinel ferrite is a very promising candidate for understanding and controlling the magnetic properties of nanoparticles at the atomic level. Moreover, they can be used in information storage, electronic devices, drug delivery, ferrofluid in sealing, biosensing and MRI technology with tunable magnetic properties [2–7]. Several methods, including coprecipitation, microemulsion, solid state reaction and other techniques [8–13] have been used to synthesize ferrite nanoparticles. Sol–gel method is an effective way to prepare magnetic nanoparticles. The citric acid and polyacrylic acid as the chelating agents in the synthesis of spinel ferrites have been reported [14,15]. In this paper, no dispersant or ammonia were used and a single citric acid was introduced in order to synthesize MFe_2O_4 nanoparticles with a simple and effective way. This method has low cost and can be conducted at low temperatures. Besides we can grow MFe_2O_4 magnetic nanoparticles with different magnetic performances by adjusting the calcination temperature. In this work we have investigated the magnetic properties of $MnFe_2O_4$ nanoparticles treated at different calcination temperatures (from 450 to 700 °C). The saturation magnetization, coercivity and magnetic susceptibility measured at room temperature (or liquid nitrogen temperature) were verified for different samples and the cation distributions in the magnetic oxides were determined by Mössbauer technique, which provide us a better understanding of cation distribution and magnetic interaction in such magnetic oxides at the atomic level.

2. Experimental

Our experimental procedure is detailed in Ref. [11]. Stoichiometric Fe^{3+}, Mn^{2+} ions and citric acid were put into the distilled water under vigorous stirring, and the resulting solution was evaporated to form the gel, which was subsequently dried until it formed the flakes (as shown in Fig. 1). The flakes were calcined under nitrogen atmosphere and the $MnFe_2O_4$ nanoparticles with different sizes were obtained. The Differential Thermal and Thermo-Gravimetric analyses were performed using differential scanning calorimeter. Powder X-ray diffraction patterns of the magnetic nanoparticles were obtained on X-ray diffractometer with Cu K_α radiation (λ=1.5418 Å). The hysteresis loop, initial magnetization curves of the samples were characterized by vibrating sample magnetometer at room temperature (as well as liquid nitrogen temperature). Mössbauer spectra were collected at room temperature on an MS-500 Mössbauer spectrometer using ^{57}Co source in a rhodium matrix, whereas α-Fe was used for calibration.

* Corresponding author.
E-mail addresses: lengjs@hit.edu.cn, ljj8081@gmail.com (J. Leng).

0304-8853/$ - see front matter Crown Copyright © 2010 Published by Elsevier B.V. All rights reserved.
doi:10.1016/j.jmmm.2010.06.035

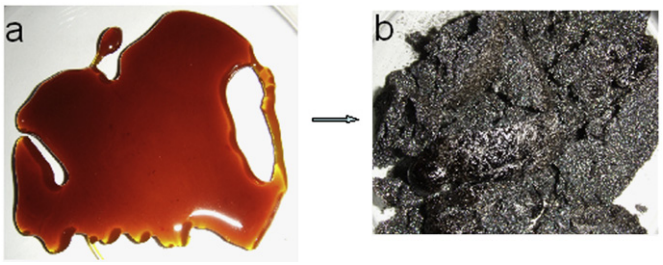

Fig. 1. Gel (a) and flakes (b) as obtained with our sol–gel growth method.

3. Results and discussion

In order to investigate the growth process of $MnFe_2O_4$ nanoparticles, differential thermal and thermo-gravimetric analyses (TGA-DTA) of the flakes obtained were carried out from 30 to 1000 °C. The results are shown in Fig. 2. The TGA curve shows a single major weight loss ending up at 400 °C and correspondingly the DTA curve exhibits an exothermic peak at the same temperature. The TGA–DTA results indicate that the flakes undergo a physical transformation and $MnFe_2O_4$ nanoparticles form at 400 °C. In the temperature ranging from 400 to 1000 °C, no weight loss and exothermic peak are present in the TGA–DTA curves. No phase transformation is observed once the spinel ferrite forms in our growth process.

Fig. 3 displays the powder X-ray diffraction patterns of the magnetic nanoparticles calcined at different temperatures. It is observed that the diffraction peaks of the samples are broadened. According to the Debye–Scherrer formula $d = K\lambda/(B\cos\theta)$, where K is a dimensionless constant and its value is 0.94 for cubic three-dimensional crystal, λ the X-ray wavelength, B the full-width at half-maximum of the diffraction peak and θ corresponds to the Bragg angle for diffraction peak, we can estimate the particle size of the samples from the (3 1 1) diffraction peaks as follows: 16 nm for 450 °C, 17 nm for 500 °C and 31 nm for 700 °C. Fig. 3 shows that the diffraction peaks of the $MnFe_2O_4$ nanoparticles treated at 450 or 500 °C are more broadened than those of the powders calcined at 700 °C. When the calcination temperature increases to 700 °C, the X-ray diffraction pattern coincides exactly with the standard spinel ferrite one (as shown with peak identification). The appearance of the (1 1 3) peak due to α-Fe_2O_3 indicates that α-Fe_2O_3 may form at the higher calcination temperatures.

Room-temperature Mössbauer spectra of the synthesized samples are investigated to understand the relationship between the magnetic performance and the cation distribution in our obtained magnetic oxides. The black dots in Fig. 4 represent the experimental data. The line through the data points is the result of the least-squares fit to the experimental data and other lines above the data correspond to individual component lines. The Mössbauer hyperfine parameters are listed in Table 1. The doublet pattern of the samples calcined at 450 and 500 °C in Fig. 4 indicates that the particles exhibit superparamagnetism. Two sexsets appear along with a doublet in the Mössbauer curves corresponding to samples obtained at 700 °C. The sexsets originating from magnetic splitting are dominant according to fractional area (only 8.8% area ratio for doublet). Distribution of Fe^{3+} ions on the tetrahedral and octahedral sites is determined from the relative area covered by the sexsets and the results can be seen in Table 1. From the results we infer that a higher calcination temperature helps Mn^{2+} ions enter into the octahedral sites while simultaneously Fe^{3+} ions transfer from the octahedral sites to the tetrahedral sites. When the samples are calcined at 450 °C, 42.5% Fe^{3+} ions occupy the octahedral sites and the

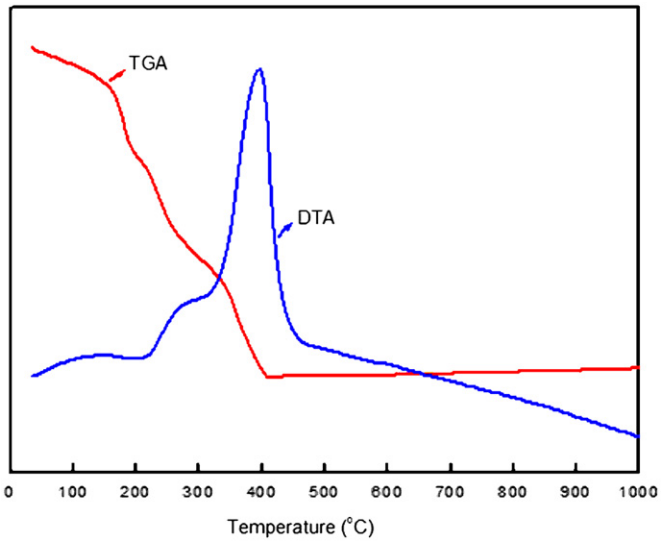

Fig. 2. TGA–DTA curves of the grown flakes: TGA (red) and DTA (blue). Temperature ranges from 30 to 1000 °C. (For interpretation of the references to color in this figure legend, the reader is referred to the web version of this article.)

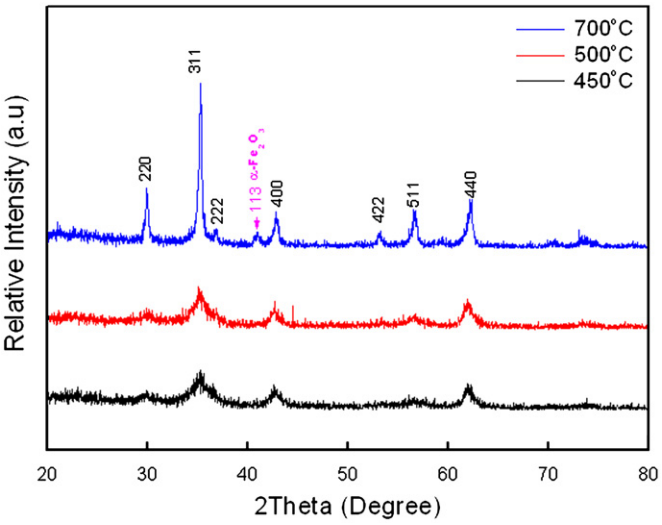

Fig. 3. Powder X-ray diffraction patterns of the prepared magnetic nanoparticles calcined at 450, 500 and 700 °C.

occupation ratio of Fe^{3+} ions at the octahedral sites decreases to 40% and 38.9% for the samples calcined at 500 and 700 °C, respectively.

The hysteresis loops of $MnFe_2O_4$ nanoparticles treated at 450, 500 and 700 °C are displayed in Fig. 5(a) and the maximum applied magnetic field is 6 kOe. The samples are measured at room temperature and the measured magnetization is divided by the total mass of the samples. At room temperature, the magnetization curves of the samples obtained at 450 and 500 °C show little hysteresis, while hysteresis is more obvious in the samples treated at 700 °C. The small coercivity of the $MnFe_2O_4$ nanoparticles obtained at 450 and 500 °C reveals their superparamagnetic nature, which is in line with the Mössbauer result. The results confirm that the thermal energy of the $MnFe_2O_4$ nanoparticles obtained at 450 and 500 °C can overcome the magnetocrystalline anisotropy energy at room temperature. Superparamagnetism generally occurs when the ferromagnetic or ferrimagnetic material is composed of very small

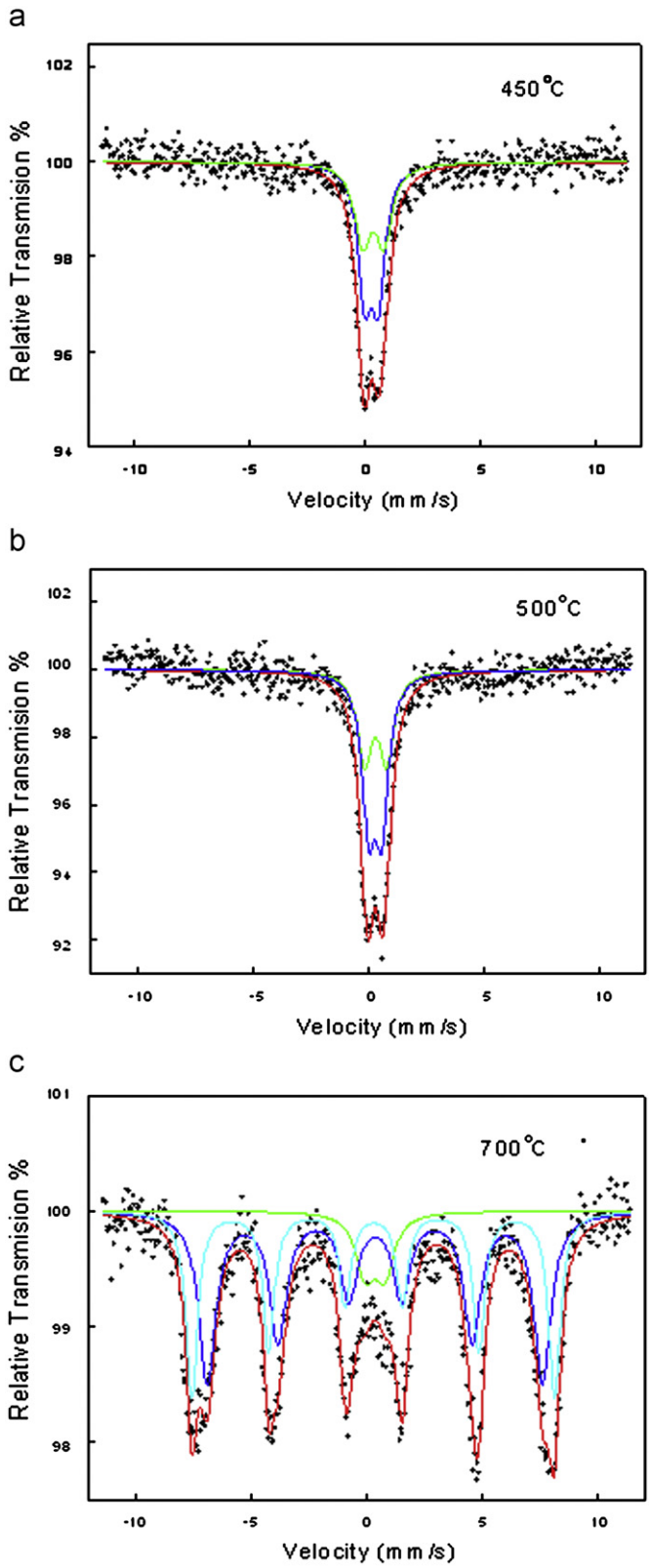

Fig. 4. Room-temperature Mössbauer spectra of the prepared magnetic nanoparticles calcined at 450 (a), 500 (b) and 700 °C (c).

Table 1
Mössbauer parameters of the prepared $MnFe_2O_4$ nanoparticles measured at room temperature.

Calcination temperature (°C)	δ (mm/s)	E_Q (mm/s)	H_{hf} (kOe)	RA (%)
450	0.41 ± 0.01	0.92 ± 0.02	–	42.5 (B)
	0.34 ± 0.01	0.59 ± 0.01	–	57.5 (A)
500	0.38 ± 0.01	0.95 ± 0.02	–	40.0 (B)
	0.37 ± 0	0.57 ± 0.01	–	60.0 (A)
700	0.40 ± 0.05	0.83 ± 0.08	–	8.8
	0.33 ± 0.01	0.02 ± 0.02	485.7 ± 0.8	38.9 (B)
	0.34 ± 0.01	0.01 ± 0.01	448.2 ± 0.6	52.3 (A)

δ, isomer shift relative to α-Fe; E_Q, quadrupole shift; H_{hf}, hyperfine field; RA, relative spectra area at A and B sites.

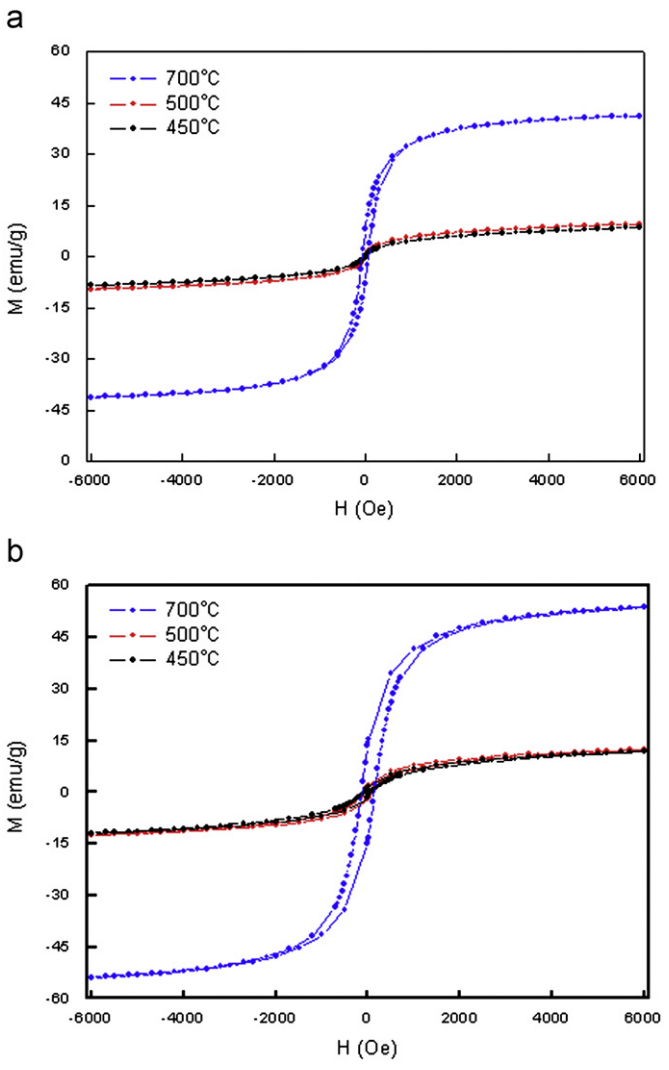

Fig. 5. Hysteresis loops of $MnFe_2O_4$ nanoparticles measured at room temperature (a) and liquid nitrogen temperature (b).

crystallites. If the temperature is below the magnetic ordering temperature, thermal energy is sufficient to change the direction of magnetization of the entire crystallite. Thus, the hysteresis loops display a remnant magnetization and a coercivity then can be very close to zero. This phenomenon is often observed when the magnetic particle size decreases to nanometers and the magnetic anisotropy energy that keeps the magnetic moment along certain directions is comparable to the thermal fluctuation energy. When the calcination temperature increases to 700 °C, the nanoparticle coercivity increases to about 68 Oe (see Table 2).

Table 2
Magnetic parameters of the prepared $MnFe_2O_4$ nanoparticles measured at room temperature.

Calcination temperature (°C)	Coercivity (Oe)	Saturation magnetization (emu/g)	Initial susceptibility (10^{-2} emu/g/Oe)
450	10	8.5	4.6
500	10	9.5	7.6
700	68	41.5	15.5

Table 3
Magnetic parameters of the prepared $MnFe_2O_4$ nanoparticles measured at liquid nitrogen temperature.

Calcination temperature (°C)	Coercivity (Oe)	Saturation magnetization (emu/g)	Initial susceptibility (10^{-2} emu/g/Oe)
450	75	12	14.2
500	95	12.5	9.8
700	143	53.8	17.1

The Stoner–Wohlfarth theory is used to describe the magnetocrystalline anisotropy energy E_A of a single-domain particle

$$E_A = KV\sin^2\theta \quad (1)$$

where K is the magnetocrystalline anisotropy constant, V the volume of the particle and θ the angle between the magnetic moment direction and the easy axis [16]. Let us first discuss the magnetocrystalline anisotropy constant in these materials. In the spinel ferrites, the AA interaction is 10 times weaker than the AB and BB interactions. $Fe_A^{3+}-Fe_B^{3+}$ exchange interaction is 2 times stronger than $Mn_A^{2+}-Fe_B^{3+}$ exchange interaction and interactions between the ions on the B site can be neglected [17]. $MnFe_2O_4$ has the near normal spinel structure $[Mn_{0.8}^{2+}Fe_{0.2}^{3+}][Fe_{1.8}^{3+}Mn_{0.2}^{2+}]O_4$. Mössbauer results of our prepared samples reveal that more Mn^{2+} ions enter into the octahedral sites and Fe^{3+} ions transfer from the octahedral sites to the tetrahedral sites. Thus the magnetocrystalline anisotropy constant of the synthesized nanoparticles should increase. The particle size of the prepared samples is much smaller than the reported value of the single domain size of spinel ferrite (~70 nm) [18,19]. Increase in the magnetic particle size with higher calcination temperature will result in higher magnetocrystalline anisotropy energy. Compared to the change in the cation distribution in the synthesized samples, increase in the coercivity with increase in calcination temperature is mostly attributed to the larger particle size.

The $MnFe_2O_4$ nanoparticles obtained at 450 and 500 °C have saturation magnetization of 8.5 and 9.5 emu/g, respectively. The samples calcined at 700 °C have the highest saturation magnetization of 41.5 emu/g among the three prepared samples. The saturation magnetization of our samples are smaller than that (80 emu/g) of bulk $MnFe_2O_4$ materials [20,21]. Saturation magnetization usually decreases with decrease in particle size due to spin canting occurring in the disordered surface layer, so the saturation magnetization of the samples calcined at 450, 500 and 700 °C increases with increase in particle size. Besides, disorder in magnetic moment orientation in the samples will result in dispersion in the exchange constant and the saturation magnetization is suppressed. Bulk $MnFe_2O_4$ has two magnetic sublattices (A and B sites in AB_2O_4 structure) separated by oxygen atoms. The magnetic interaction between A and B sites is superexchange interaction mediated by oxygen anions. The magnetic moments have ferrimagnetic alignment between A and B sublattices. Neutron diffraction has unveiled a mixed spinel structure of $MnFe_2O_4$ [22], that is to say, Mn^{2+} and Fe^{3+} ions coexist in the two sublattices. When the calcination temperature increases from 450 to 700 °C, the occupation ratio of Fe^{3+} ions at the octahedral sites decreases from 42.5% to 38.9% and this can lead to an increase in the net magnetic moment. However, the particle size is the major factor affecting the saturation magnetization in our experiments. Considering the hysteresis loops measured at 77 K (liquid nitrogen temperature) and the results shown in Fig. 5(b), the coercivity and saturation magnetization of the nanoparticles (in Table 3) increase in comparison with the values measured at room temperature and all the samples display hysteresis. For all samples, an increase in the saturation magnetization measured at 77 K results from the decrease in the thermal energy.

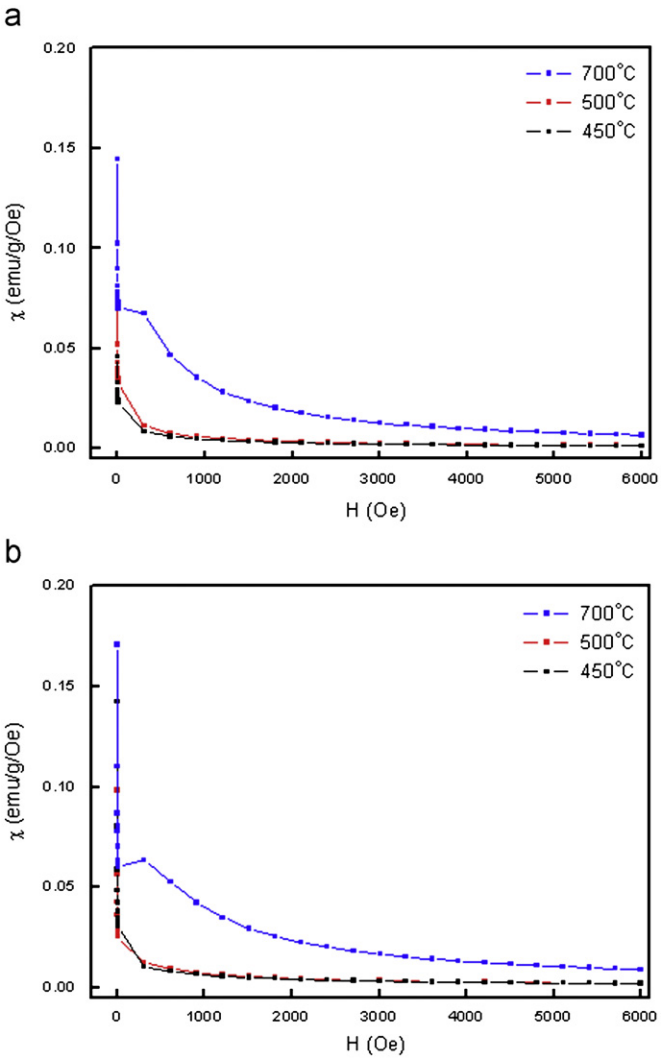

Fig. 6. Magnetic susceptibility evaluated from the initial magnetization curve of $MnFe_2O_4$ nanoparticles measured at room temperature (a) and liquid nitrogen temperature (b).

We also measured the initial magnetization curve and evaluated the magnetic susceptibility from it. The results measured at room temperature are shown in Fig. 6(a). We then infer that the initial magnetic susceptibility increases with increase in calcination temperature from 450 to 700 °C. For all samples, the maximum magnetic susceptibility appears once the magnetic field is applied. The magnetic susceptibility dependence on the magnetic field measured at 77 K is presented in Fig. 6(b).

Previously [23], it was reported that the particle interaction can reduce the initial magnetic susceptibility. We find that the initial magnetic susceptibility of the three samples measured at 77 K increases compared to that measured at room temperature. This fact means that the particle's interaction is weakened. At low temperatures, the thermal fluctuation effect on the magnetocrystalline energy of the particles is reduced and the magnetic moments will stay along certain directions resulting in weak interactions among particles. Furthermore we observe an increase in the initial magnetic susceptibility at 77 K. A shoulder is present in the magnetic susceptibility curve versus temperature for the samples obtained at 700 °C with corresponding magnetic field of 300 Oe. In effect, when the magnetic field is about 300 Oe, the magnetic moment orientation becomes unstable and abrupt switching of magnetic moment can occur according to Stoner–Wohlfarth theory.

4. Conclusion

We prepared $MnFe_2O_4$ nanoparticles using a simple, effective and low cost sol–gel method. The cation distribution was determined by Mössbauer spectroscopy. The saturation magnetization, coercivity and magnetic susceptibility measured at room temperature (and liquid nitrogen temperature) were investigated. The obtained results can help us have a better understanding of the cation distribution and size-dependent magnetic properties in such magnetic oxides at the atomic level.

Acknowledgment

This project is supported by Development Program for Outstanding Young Teachers (no. HITQNJS2009004) and Opening Funding of Key-laboratory of Special Environment Composite in Science and Technology for National Defense (no. HIT.KLOF.2009029) in Harbin Institute of Technology.

References

[1] R.C. O'Handley, in: Modern Magnetic Materials—Principles and Applications, John Wiley & Sons, New York, 2000, pp 126–132.
[2] V. Skumryev, S. Stoyanov, Y. Zhang, G. Hadjipanayis, D. Givord, J. Nogués, Nature. 423 (2003) 850.
[3] K. Raj, R. Moskowitz, R. Casciari, J. Magn. Magn. Mater. 149 (1995) 174.
[4] M. Sugimoto, J. Am. Ceram. Soc. 82 (1999) 269.
[5] K.E. Scarberry, E.B. Dickerson, J.F. McDonald, Z.J. Zhang, J. Am. Chem. Soc. 130 (2008) 10258.
[6] D.G. Mitchell, J. Magn. Reson. Imaging 7 (1997) 1.
[7] P.J. Van der Zaag, A. Noordermeer, M.T. Johnson, P.E. Bongers, Phys. Rev. Lett. 68 (1992) 3112.
[8] S.R. Ahmed, S.B. Ogale, G.C. Papaefthymiou, R. Ramesh, P. Kofinas, Appl. Phys. Lett. 80 (2002) 1616.
[9] J.A. López Pérez, M.A. López Quintela, J. Mira, J. Rivas, S.W. Charles, J. Phys. Chem. B. 101 (1997) 8045.
[10] J.P. Chen, C.M. Sorensen, K.J. Klabunde, G.C. Hadjipanayis, E. Devlin, A. Kostikas, Phys. Rev. B 54 (1996) 9288.
[11] J.J. Li, W. Xu, H.M. Yuan, J.S. Chen, Solid State Commun. 131 (2004) 51.
[12] S. Ammar, A. Helfen, N. Jouini, F. Fiévet, I. Rosenman, F. Villain, P. Molinié, M. Danot, J. Mater. Chem 11 (2001) 186.
[13] A. Goldman, in: Modern Ferrite Technology, 2nd ed., Springer, 2006, pp 172–173.
[14] Z.X. Yue, J. Zhou, L.T. Li, H.G. Zhang, Z.L. Gui, J. Magn. Magn. Mater. 208 (2000) 55.
[15] D.H. Chen, X.R. He, Mater. Res. Bull. 36 (2001) 1369.
[16] D.L. Leslie-Pelecky, R.D. Rieke, Chem. Mater. 8 (1996) 1770.
[17] P.J. Van Der Zaag, A. Noordermeer, M.T. Johnson, B.F. Bongers, Phys. Rev. Lett. 68 (1992) 3112.
[18] A. Berkowitz, W.T. Schuele, J. Appl. Phys. 30 (1959) 134S.
[19] S. Yáñez-Vilar, M. Sánchez-Andújar, C. Gómez-Aguirre, J. Mira, M.A. Señarís-Rodríguez, S. Castro-García, J. Solid State Chem. 182 (2009) 2685.
[20] Z.X. Tang, C.M. Sorensen, K.J. Klabunde, G.C. Hadjipanayis, Phys. Rev. Lett. 67 (1991) 3602.
[21] M. Niederberger, G. Garnweitner, Chem. Eur. J. 12 (2006) 7282.
[22] C. Liu, B.S. Zou, A.J. Rondinone, Z.J. Zhang, J. Phys. Chem. B. 104 (2000) 1141.
[23] R.W. Chantrell, N.S. Walmsley, J. Gore, M. Maylin, J. Magn. Magn. Mater. 196–197 (1999) 118.